Advanced Composite Materials
Publication details, including instructions for authors and subscription information:
http://www.tandfonline.com/loi/tacm20

Interfacial Evaluation and Self-Sensing of Single Micro-Carbon Fiber/CNF-Brittle-Cement Composites using Electro-Micromechanical Tests and Acoustic Emission

Joung-Man Park [a] , Pyung-Gee Kim [b] , Zuo-Jia Wang [c] , Dong-Jun Kwon [d] & K. Lawrence De vries [e]

[a] School of Materials Science and Engineering, Engineering Research Institute, Gyeongsang National University, Jinju 660-701, Korea; Department of Mechanical Engineering, The University of Utah, Salt Lake City, Utah 84112, USA;, Email: jmpark@gnu.ac.kr

[b] School of Materials Science and Engineering, Engineering Research Institute, Gyeongsang National University, Jinju 660-701, Korea

[c] School of Materials Science and Engineering, Engineering Research Institute, Gyeongsang National University, Jinju 660-701, Korea

[d] School of Materials Science and Engineering, Engineering Research Institute, Gyeongsang National University, Jinju 660-701, Korea

[e] Department of Mechanical Engineering, The University of Utah, Salt Lake City, Utah 84112, USA

Version of record first published: 02 Apr 2012.

VSP

Advanced Composite Materials 20 (2011) 149–168

ADVANCED COMPOSITE MATERIALS
brill.nl/acm

Interfacial Evaluation and Self-Sensing of Single Micro-Carbon Fiber/CNF–Brittle-Cement Composites using Electro-Micromechanical Tests and Acoustic Emission

Joung-Man Park [a,b,*], **Pyung-Gee Kim** [a], **Zuo-Jia Wang** [a], **Dong-Jun Kwon** [a] **and K. Lawrence DeVries** [b]

[a] School of Materials Science and Engineering, Engineering Research Institute, Gyeongsang National University, Jinju 660-701, Korea

[b] Department of Mechanical Engineering, The University of Utah, Salt Lake City, Utah 84112, USA

Received 14 June 2009; accepted 29 June 2010

Abstract

Interfacial evaluation and self-sensing were investigated for single carbon fiber/carbon nanofiber (CNF)–brittle-cement composites by electro-micromechanical techniques and acoustic emission (AE) under cyclic loading/subsequent unloading. During the curing process, the volumetric resistivity decreased dramatically, during the initial stage, due to increased contact points between the cement matrix and the CNF. The apparent modulus and electrical contact resistivity of micro-carbon fiber/CNF–cement composites were also evaluated as a function of CNF concentration. As the CNF concentration increased, the maximum stress increased, whereas the change in resistance $\Delta\rho$ decreased gradually and the contact resistivity sensitivity increased as well. Micro-damage sensing of micro-carbon fiber/CNF–cement composites was also investigated by electrical resistivity and AE. When the first fracture of micro-carbon fiber occurred, the electrical resistivity increased 'infinitely' with increasing lower CNF concentrations. For high 5 wt% CNF, however, the fracture of micro-carbon fiber could be detected just in one large step increment change in the electrical resistivity as well as consistent AE events. The percolation structure of CNF is not well formed in the cement matrix due to relatively-low electrical conductivity. The chosen CNF–cement composites are not suitable for conductive and sensing applications because of their many vertical microcracks.

Keywords

Interface/interphase, aspect ratio, micro-mechanics, acoustic emission

1. Introduction

Carbon nanofiber (CNF) is one of the greatly potential reinforcing additives for polymeric composites due to carbon nanofiber's high axial Young's modulus, high

* To whom correspondence should be addressed. E-mail: jmpark@gnu.ac.kr
Edited by the KSCM

DOI:10.1163/092430410X523962

aspect ratio, large surface area, and excellent thermal and electrical properties [1]. Among these, a particular important advantage of CNF compared to conventional fillers like carbon black and silica is its higher aspect ratio, which is important for many mechanical and electronic applications [2, 3]. It is observed experimentally that the percolation threshold strongly depends on the aspect ratio of the reinforcement. Nano-scaled additives are currently being considered as filler materials to produce high-performance structural polymer composites with significantly enhanced functional properties [4, 5]. In particular, it is well known that the degree of dispersion is one of the most important factors affecting the electrical and mechanical properties of nanocomposites.

In a ceramic material, a reinforcing effect is not as important in terms of stress transference mechanism as in polymer composites. Based on their brittleness and nonconductive nature, for these ceramics reinforcing carbon fiber can keep the total shape of the composite specimen. The reason for using a single carbon fiber is to give a simplified experimental system (although it is not a real system). Single fiber/CNF–cement composites can provide quantitative information on the interfacial adhesion. Cement structures constitute a large portion of civil infrastructures, but their reliability is relatively low because of the widely varying materials and complex service environment [6, 7]. Consequently, the safety of cement structures is an important issue in civil engineering. Although the occurrence of engineering accidents involving cement structures during their service life can be greatly reduced by careful structural design, unexpected occurrences of extreme situations can still threaten the safety of cement structures, making it necessary to monitor the state of cement structures in real time [8–10].

Cement-based composites containing carbon particles, carbon fibers, and other additives have been studied as potential new composite materials. Their outstanding physical and electrical properties make them suitable for use in technologically advanced products [11, 12]. The studies of Li *et al.* demonstrated that carbon nanotube (CNT) can act as bridges across cracks and voids thereby forming reinforcing mechanisms and crack arrestors in cement matrixes. This improves the flexural strength, compressive strength, and failure strain of cement matrix composites [13]. Carbon particles, carbon fibers, and other additives in reinforced cement composites can act as piezoresistivity strain self-sensors [14], useful for weighing, traffic monitoring, border monitoring, building room occupancy monitoring, building security structural vibration control, etc. Furthermore, the electrical conductivity induced by such fillers allows other applications as well, such as electrical grounding protection, electromagnetic interference (EMI) shielding and electrostatic discharge protection. Because of their favorable functional properties, carbon particle cement-matrix composites can be viewed as attractive multifunctional structural materials [15].

Electro-micromechanical techniques have been studied as economical nondestructive evaluation (NDE) methods for damage sensing, the characterization of interfacial properties, and nondestructive behavior in which a conductive fiber can

act as a sensor, as well as a reinforcing fiber [16, 17]. Fiber damage in an electrical-insulator matrix cannot be detected after the first micro-carbon fiber fracture occurs, whereas in an electrically conductive matrix carbon fiber fracture as well as matrix deformation can be detected continuously by electrical resistance measurement [18].

Acoustic emission (AE) is a commonly used nondestructive (NDT) testing method [19, 20]. AE has been used to monitor fracture behavior of composites structures, and to characterize AE parameters to develop a better understanding of the types of fracture sources and their progression. When tensile loading is applied to composite materials, many AE signals can occur from fiber fracture, matrix cracking, and interfacial failure. Generally, the AE energy released by fiber fracture is significantly greater than that associated with matrix cracking or debonding [21–23]. In this study, reinforcing effects, electrical resistivity and nondestructive micro-damage sensing in micro-carbon fiber/CNF–brittle-cement composites, were investigated using electro-micromechanical techniques and AE.

2. Experimental

2.1. Materials

Pyrograf III® carbon nanofiber (CNF) (grade PR-24-PS, supplied from Applied Science Inc.) was used in this study, in which the batch of Pyrograf III® was pyrolytically stripped vapor-grown CNF. Several properties for this CNF are supplied by the brochure of Applied Sciences Inc. in Table 1. CNF was used as a reinforcing as well as self-sensing elements. Another conventional micro-carbon fiber, with an average diameter of approximately 8 μm (TZ307, Taekwang Co., Korea) was also used as reinforcement and sensor. Portland cement (Type I, Tongyang Cement Corp., Korea) was used as a brittle-cement matrix. For preparing DMC (dual matrix composite) specimen, an outer matrix was made of the mixture of epoxy resin (YD-128, Kukdo Chemical Co., Korea) based on diglycidyl ether of bisphenol-A (DGEBA) and polyoxypropylene diamine curing agents (Jeffamine D-400 and D-2000, Huntzman Petrochemicals Co.).

2.1.1. Preparation of CNF/Cement Composites

Figure 1 outlines the process used in the specimen preparation of CNF–cement composite samples using sonication (Crest Ultrasonic Co.). CNF was dispersed in water based on the different weight fraction of CNF in cement composite by sonication for 12 h, and then the CNF dispersive water was mechanically mixed with cement to form a cement paste. The CNF–cement paste was composed of Portland cement and CNF dispersive water with weight ratio of 100:30. This mixture was then placed in a mold, and the CNF–cement composites were cured at 25°C, 90% relative humidity (RH) for 7 days.

Table 1.
Properties of carbon nanofiber (CNF) used in this work (from brochure of Applied Sciences Inc.)

Properties	Pyrograf III® PR-24-PS
Ultimate strength (GPa)	7.0
Tensile strength (GPa)	600
Diameter (nm)	150
Length (μm)	15
Aspect ratio (l/d)	100
Density (g/cm^3)	1.95
Electrical resistivity (μΩ · cm)	55
Elemental surface oxygen (%)	1.4

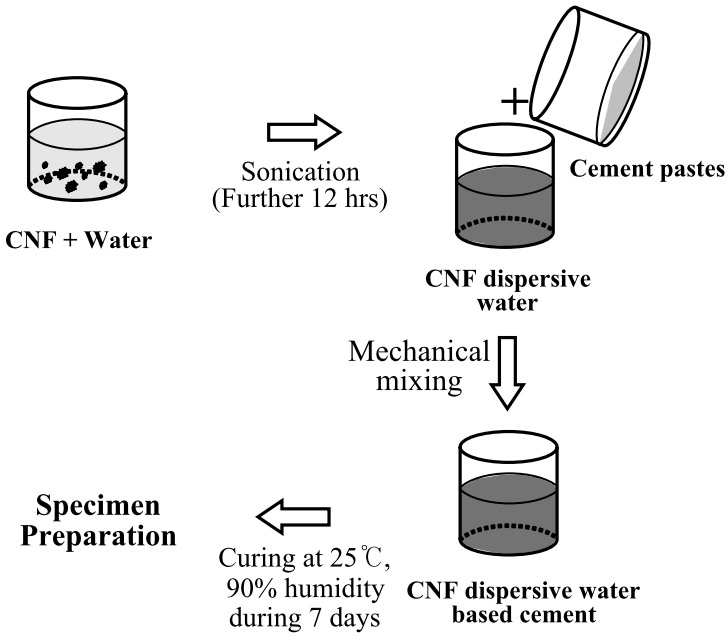

Figure 1. Outline of specimen preparation of CNF–cement composites.

2.1.2. Preparation of Dual Matrix Composites (DMC)

The DMC specimen is composed of a single fiber, a brittle layer (inner matrix for measuring interface) and a ductile matrix (supportable outside matrix). The DMC test was performed to sense the fiber fracture through the conductive inner matrix embedded carbon fiber. In the DMC test, the conductive inner matrix embedded carbon fiber was fixed in a silicone mold. After the epoxy mixture was poured into the mold, the epoxy was precured at 80°C for 2 h and then post-cured at 120°C for 2 h.

2.2. Methodologies

2.2.1. Electrical Resistance Measurements

Figure 2(a) shows the experimental setup for determination of the electrical volumetric resistivity. The electrical resistance of the CNF composites was measured by the four-point probe method. Electrical contact points were located at regular intervals along the specimen, using copper wire and silver paste. Electrical volumetric resistivity was obtained from the measured electrical volumetric resistance, the cross-sectional area of the CNF composites, specimen A_v, and the electrical contact length, L_{ec} (the spacing between the two central copper wires). The relationship between the electrical volumetric resistivity, ρ_v, and the measured electrical resistance, R_v is:

$$\rho_v = \left(\frac{A_v}{L_{ec}}\right) \times R_v. \tag{1}$$

The reinforcing effect was measured indirectly by apparent modulus, which is the modulus of single micro-carbon fiber embedded in the matrix, using uniform cyclic loading. Figure 2(b) shows the experimental specimen/setup for the measurement of the apparent modulus. Carbon fiber was fixed in a silicone mold using Scotch tape, and then the CNF–cement composite was added. The width of the specimen was 2 mm, and thickness was 1 mm. For the cyclic strain test, the strain–stress curve was determined using a universal testing machine, UTM (Hounsfield Test Equipment Ltd., U.K.) at a test speed of 0.5 mm/min and with a 100 N load cell. After fixing a testing specimen into the UTM grips, electrical connections to a multimeter (used for electrical resistance measurement) were made using copper wire. The electrical resistance of the cement nanocomposite was measured, simultaneously with measurements of the stress–strain change, while five load cycles were applied to the sample.

Figure 2(c) shows the experimental arrangement used for the electrical sensing in the electro-pullout test. During the fiber pullout test, the change in resistance, ΔR through the conductive matrix, as a function of the fiber tension, was measured by the four-probe method simultaneously. Two electrical contacts were attached to the carbon fiber and the other two electrical contacts were affixed around the whole perimeter of the cement–nanocomposite (see Fig. 2(c)). The electrical resistance between the two central voltage contacts was measured. Referring to Fig. 2(c) it can be seen that this resistance corresponds to the sum of the electrical resistances for the portion of the carbon fiber between the two voltage contacts, the electrical contact resistance, R_c, between the carbon fiber and the cement nanocomposite and the resistance of the portion of the nanocomposite between the two voltage contacts. That is, the total resistance for the electro-pullout system can be expressed as:

$$R_T = R_v^{\text{fiber}} + R_c + R_v^{\text{nanocomposites}}. \tag{2}$$

At least 3 specimens were measured for each experimental set to obtain statistically meaningful data.

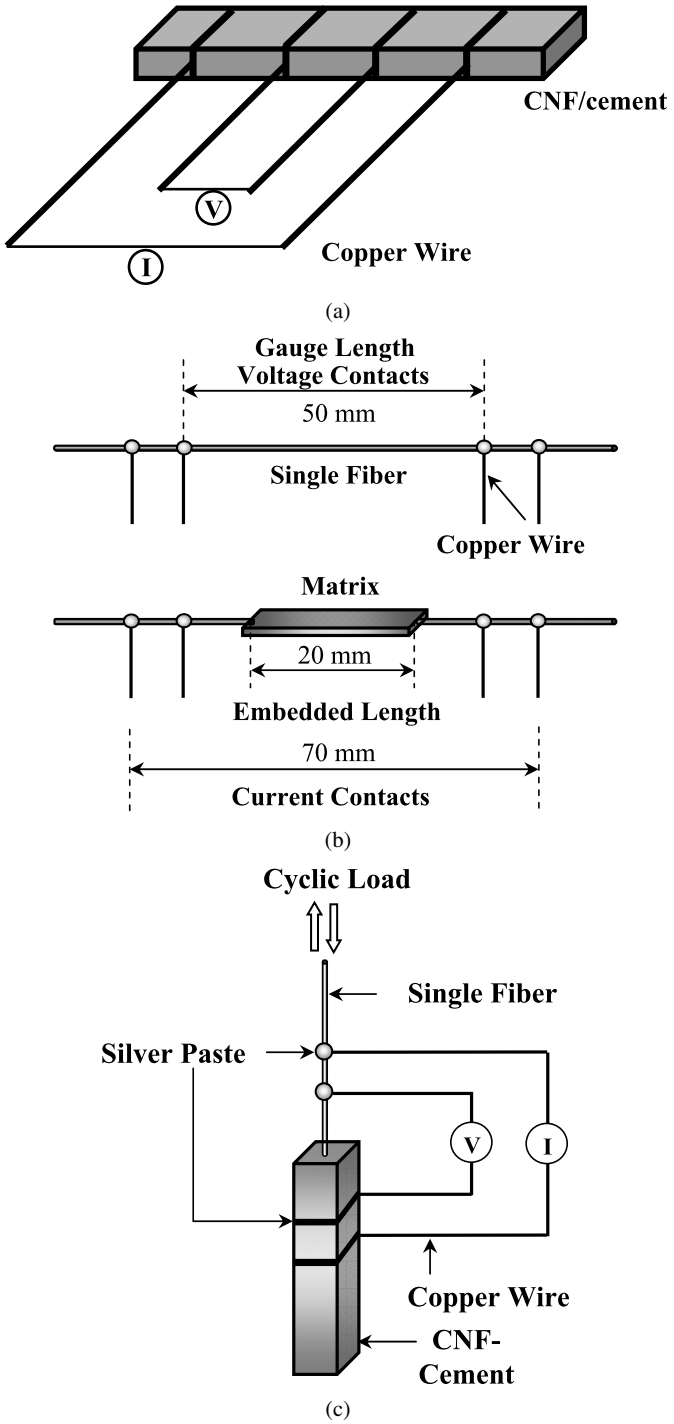

Figure 2. Experimental scheme of electrical resistance measurement for: (a) volumetric resistivity; (b) apparent modulus and (c) electro-pullout test.

2.2.2. AE Measurement

Figure 3 shows the experimental system used for damage sensing by measurements of the electrical resistance and acoustic emission (AE) (Mistras 2001 System, Physical Acoustics Co.). The DMC specimens for measuring electrical resistance and AE parameters were tested in tension in a mini-UTM (Pico Industrial Inc., Korea) with a 100 kg_f load cell at a test speed of 0.5 mm/min. The change in electrical resistance associated with fiber fracture was measured and related to the AE parameters. In an effort to determine the microfailure mechanisms in composite materials, AE tests were combined with the micromechanical tests. The test specimen was gripped in the UTM and an AE PZT sensor was attached in the center of the sample using vacuum grease for acoustic coupling. The AE signals were detected using a miniature sensor (Wide band, WD model, Physical Acoustics Co.) with a peak sensitivity

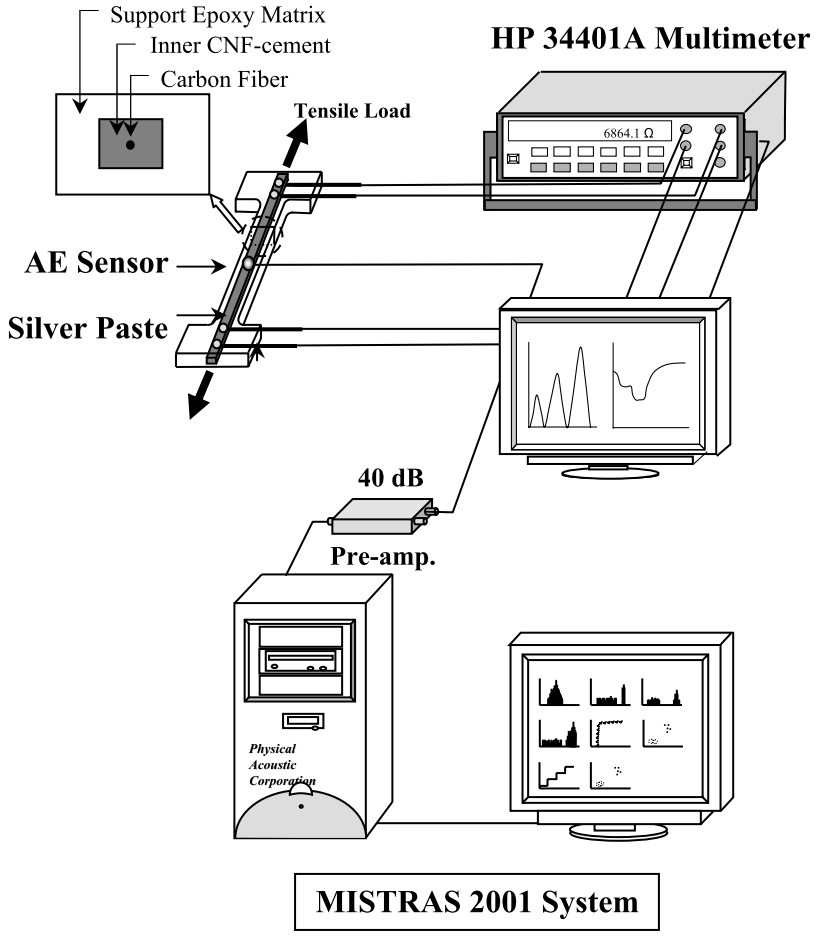

Figure 3. Experimental scheme for damage sensing using electrical resistance measurement and AE in double-matrix composites test.

of 55 Ref. V/(m/s) [−62.5 Ref. V/mbar] and a resonant frequency of 125 [650] kHz. The sensor output was amplified by 40 dB by a preamplifier and passed through a band-pass filter with a range of 100 to 1000 kHz with the threshold level set up as 40 dB. Elastic waves occurring from microfailure sources were converted to voltage signals by the PZT sensor, and then to AE parameters. Fast Fourier transform (FFT) was used to frequency-analyze the waveform and to identify the characteristic peaks of the frequency components, for the microfailure sources.

3. Results and Discussion

3.1. Self-Sensing of Single Micro-Carbon Fiber/CNF–Cement Composites

Figure 4 shows the change in volumetric resistivity, $\Delta\rho$, of a 5 wt% CNF–cement composite *versus* elapsed time, during the curing process. The volumetric resistivity decreased with elapsed time, especially during the first 40 h of cure, after which it leveled-off. It is hypothesized that this behavior is due to the contact points between the CNF particles decreasing during the curing process and evaporation of water particles [24].

Figure 5 shows the results for uniform cyclic loading tests of micro-carbon fiber/CNF–cement composites with four filler concentrations: (a) 0 wt%; (b) 1 wt%; (c) 2 wt% and (d) 5 wt%. Note that the electrical resistivity, stress and strain responded well under the five uniform loading/unloading cycles. For the cyclic strain tests represented in Fig. 5, as the CNF concentration increased, the value of the

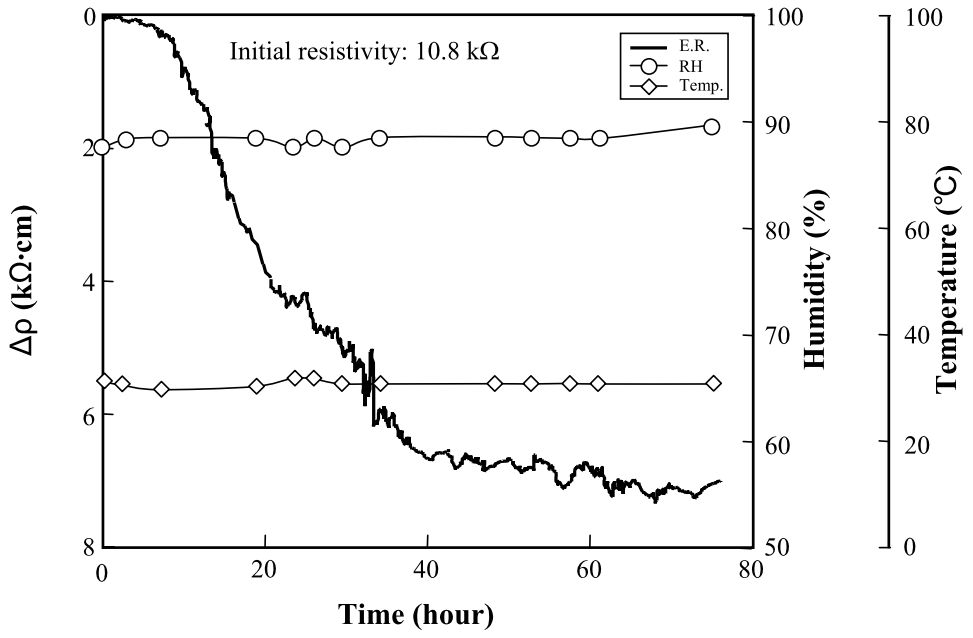

Figure 4. Volumetric resistivity for CNF 5 wt%–cement composites with elapsed time of cure.

maximum cyclic stress increased slightly. The relative decrease in the magnitude of $\Delta\rho$ with concentration was somewhat larger but still small. These tendencies could be related to the material's apparent modulus, a fact that might provide in-

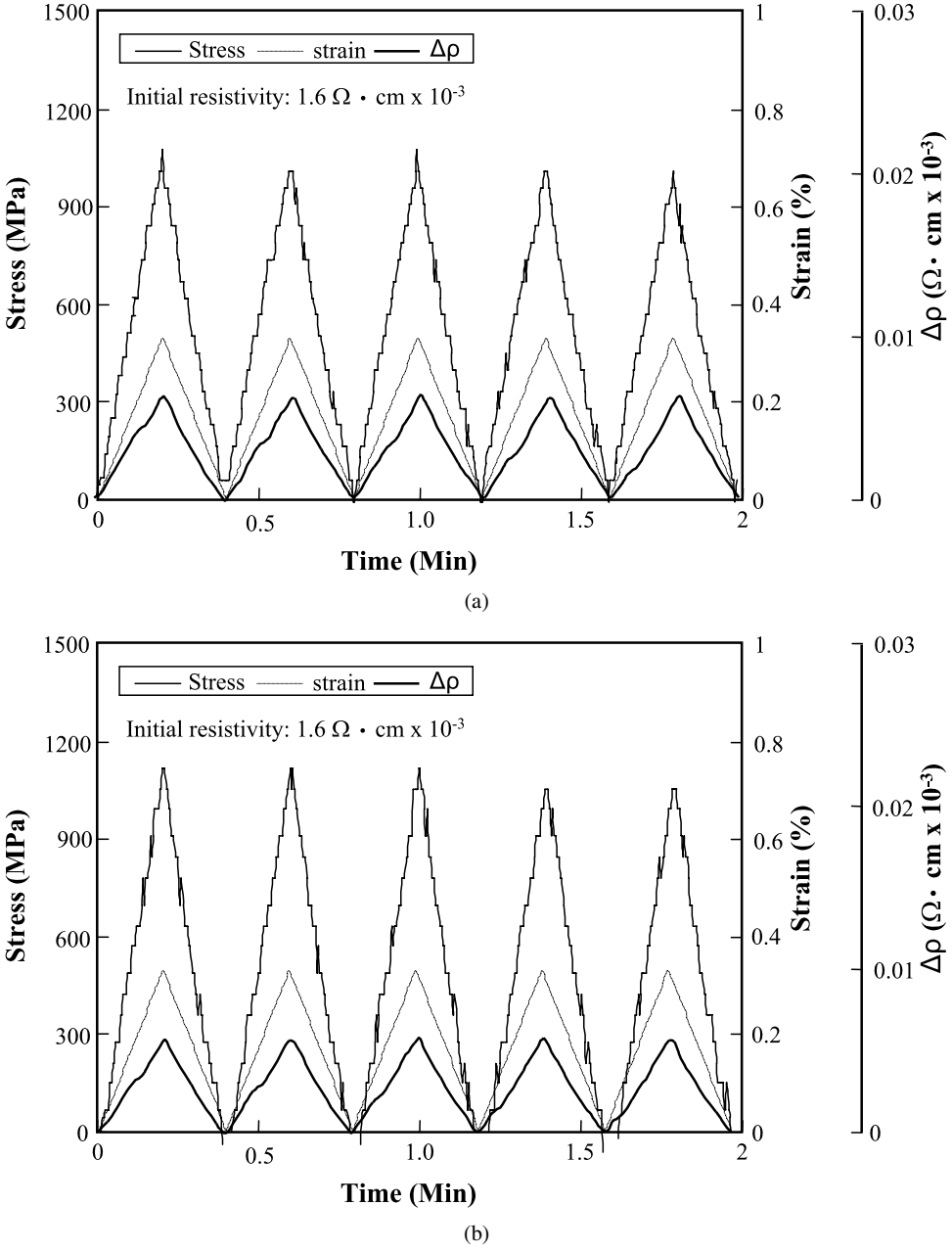

Figure 5. Uniformed cyclic loading test of micro-carbon fiber/CNF–cement composites with four concentrations: (a) 0 wt%; (b) 1 wt%; (c) 3 wt% and (d) 5 wt%.

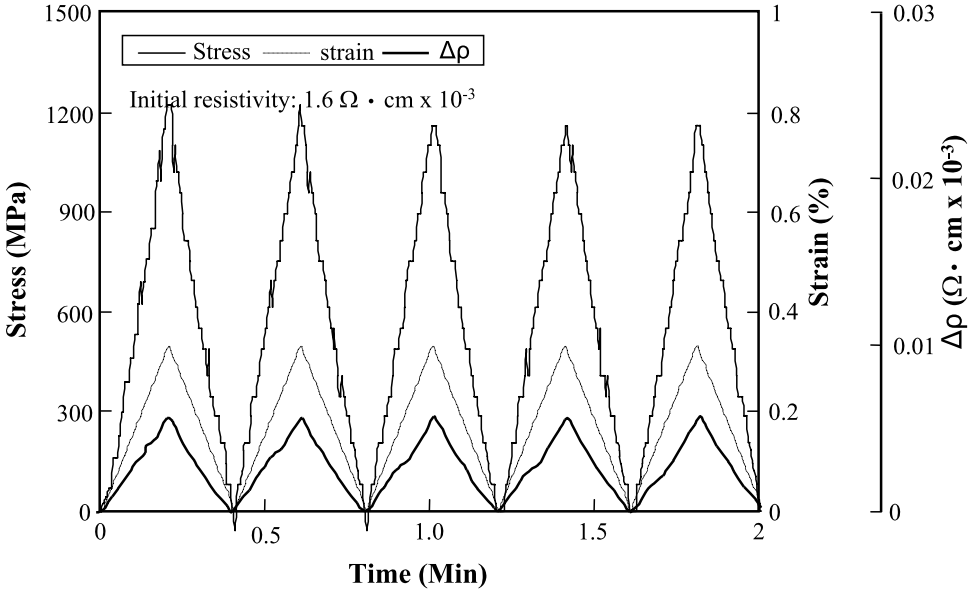

(c)

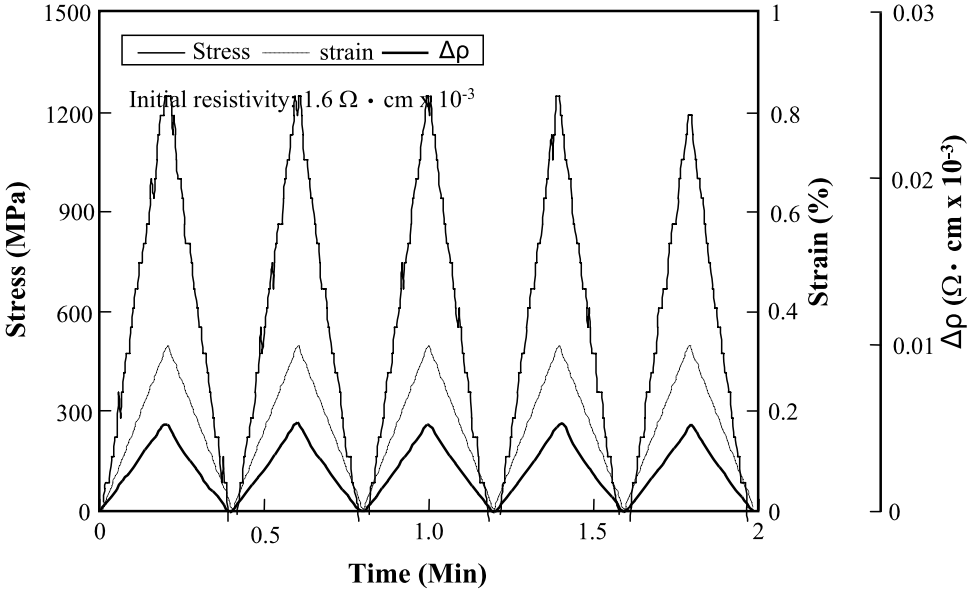

(d)

Figure 5. (Continued.)

sight into interfacial properties. As note previously, apparent modulus is the fiber modulus that is embedded in the matrix and is obtained by comparing the stress–strain curve of an embedded fiber with the modulus of carbon fiber 'itself' [25, 26]. The displacement of carbon fibers in the higher CNF concentration regime might

be more constrained due to the higher modulus of the embedded matrix. That is, at lower CNF concentrations, displacement near the interface might occur more easily due to relatively lower modulus of the CNF–cement matrix, while at higher CNF concentrations (larger relative modulus) this motion should be more difficult.

Figure 6 shows the apparent modulus and electrical resistivity of micro-carbon fiber/CNF–cement composites for different CNF concentrations. Figure 6 is separated as: (a) stress–strain curve; (b) $\Delta\rho$–strain curve and (c) apparent modulus and $\Delta\rho$. The slopes of the stress–strain curves were used to determine this apparent modulus which differed with CNF concentrations, as shown in Fig. 6(c). Note that as the apparent modulus increased, with CNF concentration, the values of $\Delta\rho$ decreased consistent with the discussion at the end of the previous paragraph.

Figure 7 shows the change in electrical contact resistivity between micro-carbon fiber and CNF–cement composites with differing CNF concentrations: (a) 0 wt%; (b) 1 wt%; (c) 3 wt% and (d) 5 wt%. Sensitivity of the contact resistivity increased with CNF, though some signals were rather electronically noisy. As might be expected, the $\Delta\rho$ for fiber loading/unloading could not be detected well in the case of 0 wt% CNF. However, since such cements typically contain electrically active ions, including those associated with water molecules, cement is not quite as good an insulator as are nonconductive polymers. For the CNF–cement composites with higher CNF concentrations under fiber loading/unloading, $\Delta\rho$ could be more easily sensed (in terms of electrical contact resistivity) with much less noise.

3.2. Nondestructive Micro-Damage Sensing of CNF–Cement Composites

Figure 8 shows the micro-damage due to micro-carbon fiber fracture in CNF–cement double matrix composites with concentration of: (a) 0 wt%; (b) 1 wt%; (c) 3 wt% and (d) 5 wt%. When the first micro-carbon fiber fracture occurred, the electrical resistivity increased very substantially ('infinitely') for composites with 0, 1, 3 wt% CNF concentrations. For 5 wt% CNF, however, the micro-carbon fiber fracture could be detected as just one step in electrical resistivity change as well as AE. However, when the second micro-carbon fiber fracture occurred, the electrical resistivity increased 'infinitely'. Since the percolation structure of CNF is typically poorly developed in cement, conductive CNF–cement composites are changed to nonconductive by vertical microcracks. Since this may be an inherent property in the less conductive CNF material, it may be that for sensing applications more conductive CNF or even CNT will be required.

Figure 9 shows typical AE waveforms and their FFT analyses for signals due to micro-damage in micro-carbon fiber/CNF–cement double-matrix composites for: (a) micro-carbon fiber fracture and (b) debonding or CNF–cement matrix cracking. Typical waveforms of micro-carbon fiber failure were observed to have large amplitude, whereas the interfacial failure between micro-carbon fiber and cement matrix exhibited much smaller amplitudes. The FFT patterns for micro-carbon fiber failure were different from those associated with debonding or CNF–cement matrix cracking. Although there may be AE events occurring from brittle-cement matrix

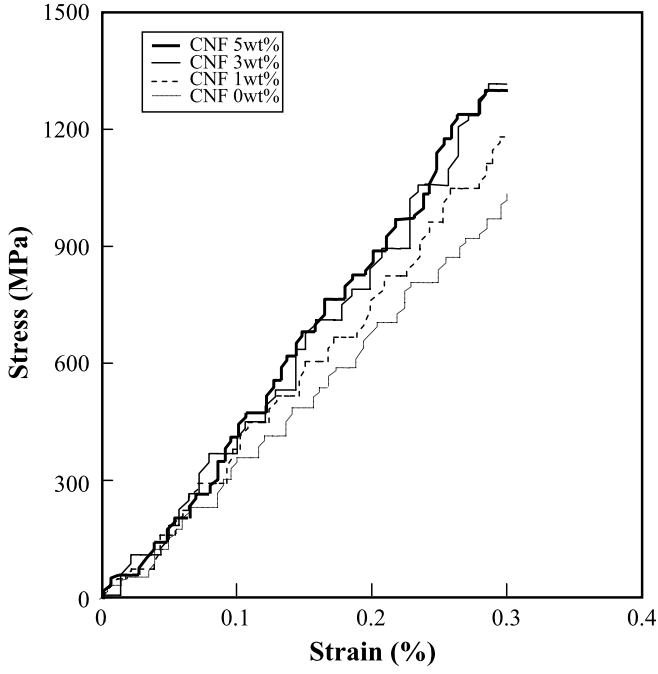

(a)

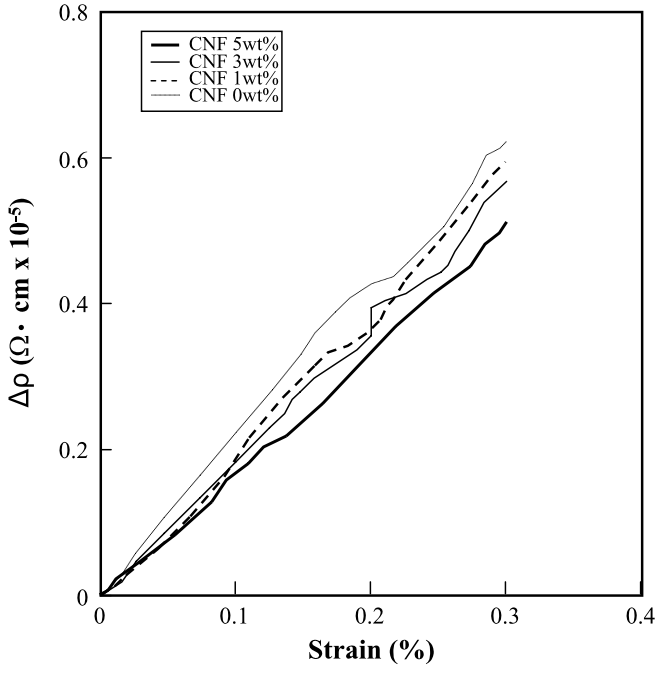

(b)

Figure 6. Apparent modulus and electrical resistivity of micro-carbon fiber/CNF–cement composites with concentrations of: (a) stress–strain curve; (b) $\Delta\rho$–strain curve and (c) apparent modulus and $\Delta\rho$.

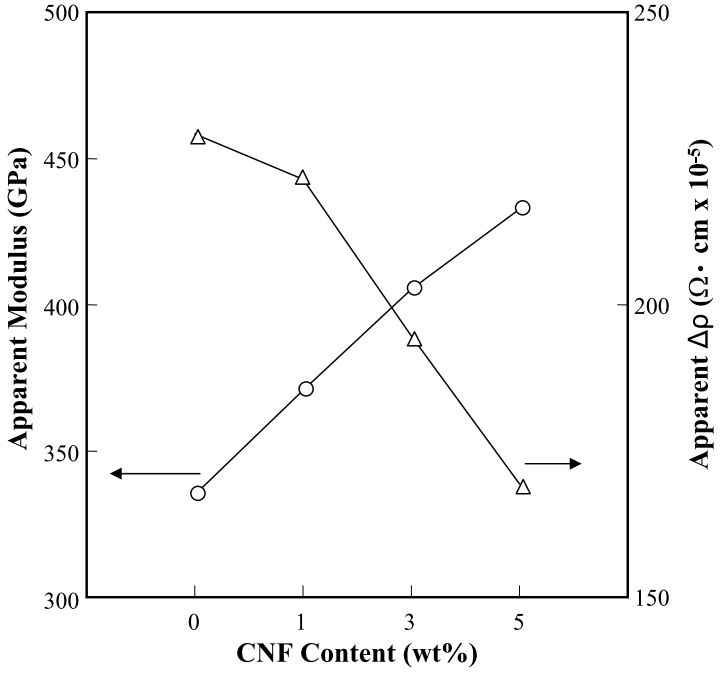

(c)

Figure 6. (Continued.)

cracking, it would be rather difficult to distinguish either cement matrix cracking or micro-carbon fiber fracture due to their similar AE energy and amplitude [20].

Figure 10 shows photographs of vertical microcracks after AE tests of micro-carbon fiber/CNF–cement double-matrix composite with CNF concentrations of: (a) 0 wt%; (b) 1 wt%; (c) 3 wt% and (d) 5 wt%. Vertical multiple microcracks were observed after tensile tests due to the inherent nature of brittle and strong cement matrixes, which significantly affects the electrical conductivity. The number of vertical cracks did not appear to be significantly affected by CNF content except; in general, the number appeared to be less compared to the case for no CNF addition. It might be that the addition of CNF affects the blunting of vertical cracking through energy absorption, which may result in a reduced number of vertical cracks in a brittle-cement matrix.

4. Conclusions

The change in electrical resistivity of single micro-carbon fiber/CNF–cement composites with CNF concentration was investigated for measuring load and micro-damage sensing combined with micromechanical techniques. Volumetric resistivity decreased dramatically at the initial curing stage and then leveled-off with elapsed

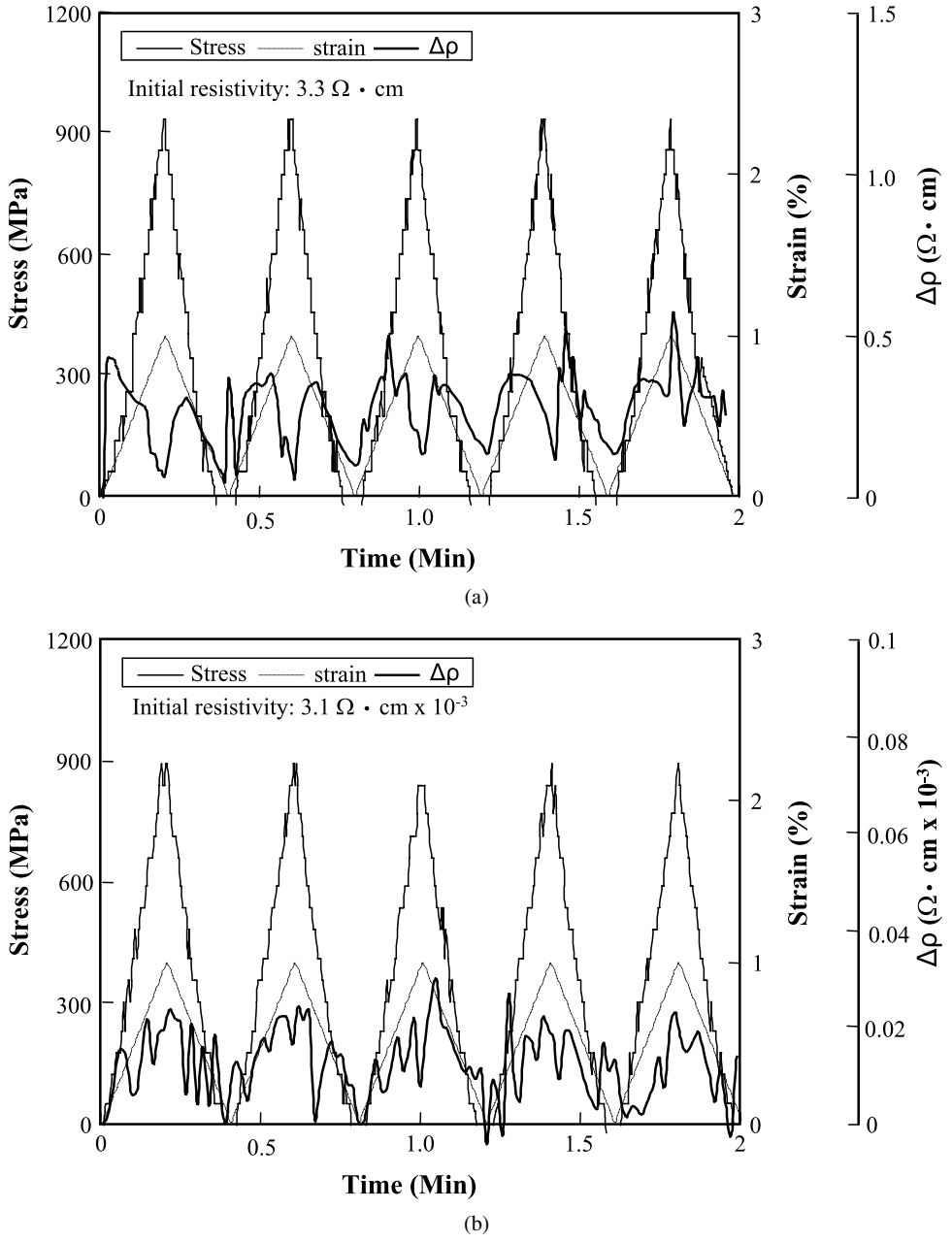

Figure 7. The change in electrical contact resistivity of between micro-carbon fiber and CNF–cement composites with concentrations of: (a) 0 wt%; (b) 1 wt%; (c) 3 wt% and (d) 5 wt%.

time during curing. Electrical volumetric resistivity of CNF–cement pastes was difficult to measure below 3 wt% CNF due to low conductivity of the CNF itself. Electrical resistivity responded well under uniform cyclic loading. These tenden-

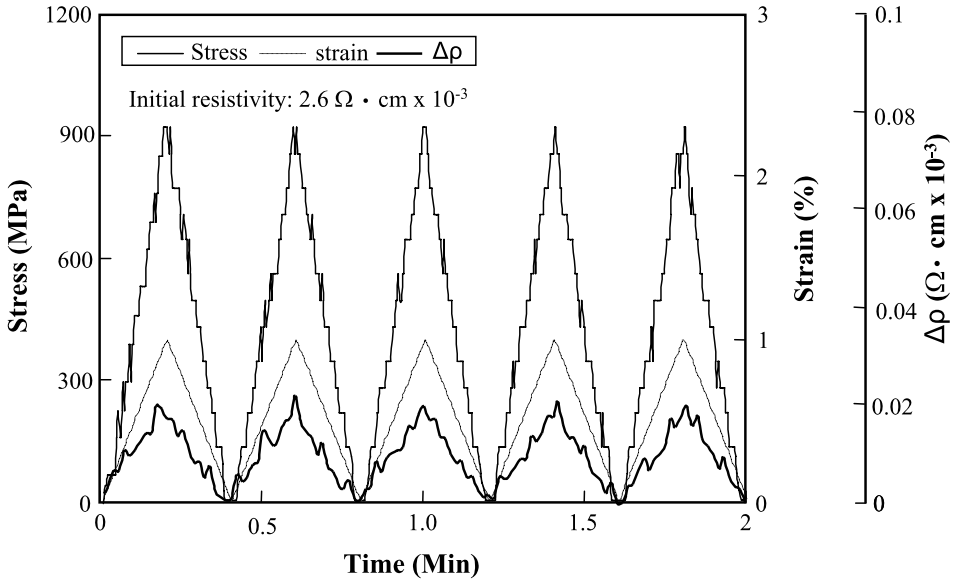

(c)

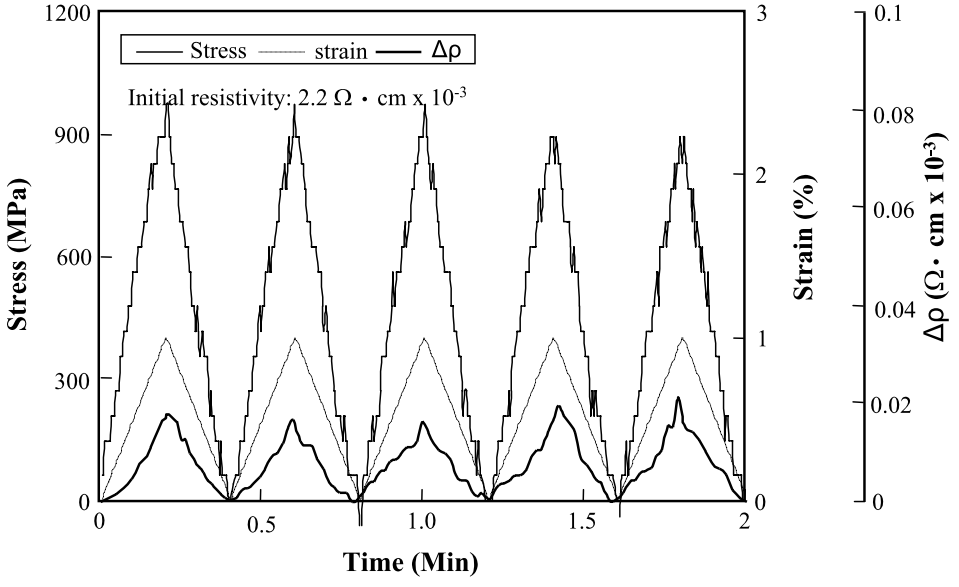

(d)

Figure 7. (Continued.)

cies could be related to changes in the composite apparent modulus, which can provide some information on interfacial bonding. Sensitivity of contact resistivity increased with CNF concentration by reducing signal noise.

For micro-damage sensing, when the first micro-carbon fiber fracture occurred, the electrical resistivity increased 'infinitely' for low CNF concentrations. For high

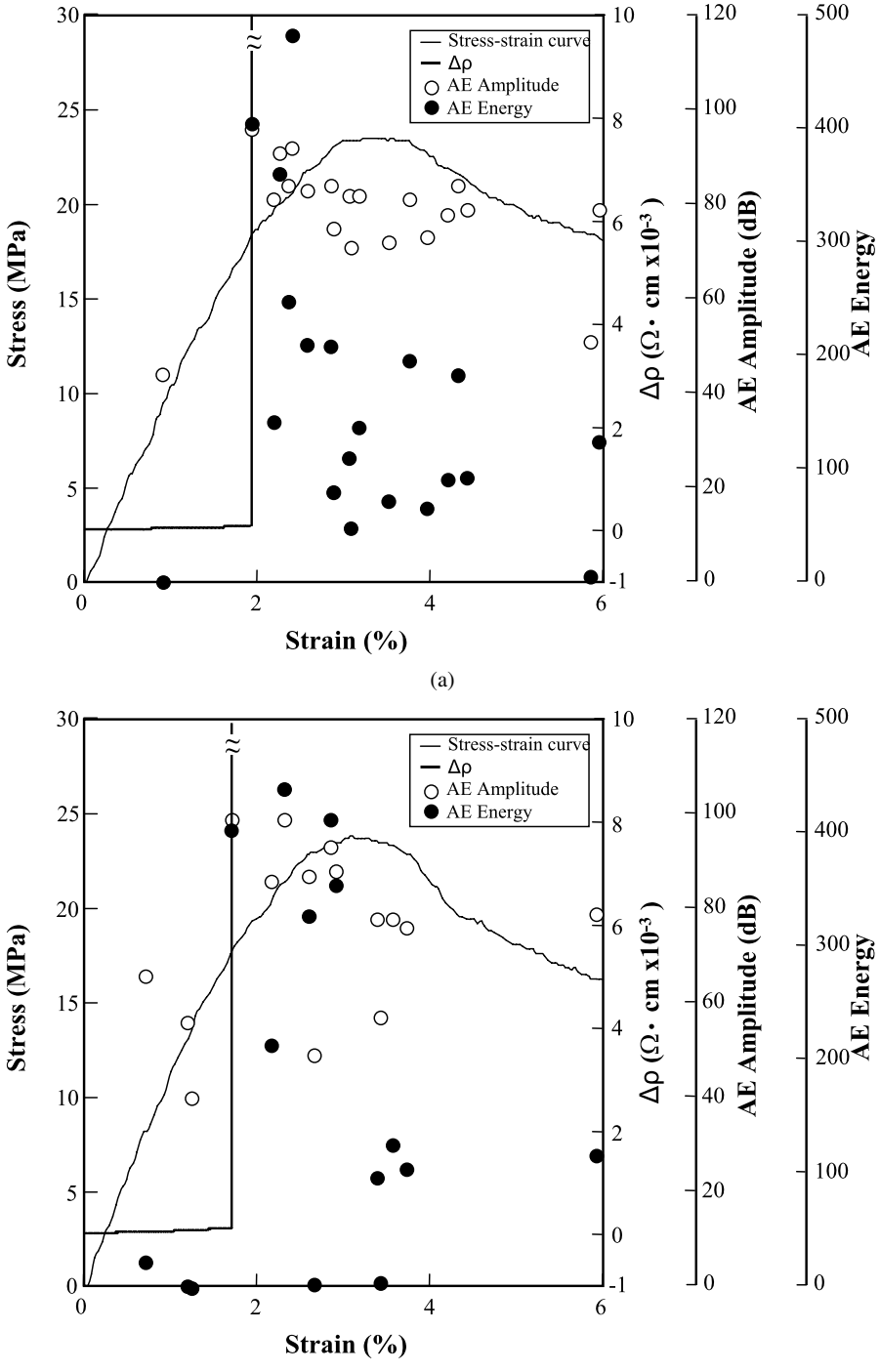

Figure 8. Damage sensing of micro-carbon fiber fracture for CNF–cement double-matrix composites with concentration of: (a) 0 wt% CNF; (b) 1 wt% CNF; (c) 3 wt% CNT and (d) 5 wt%.

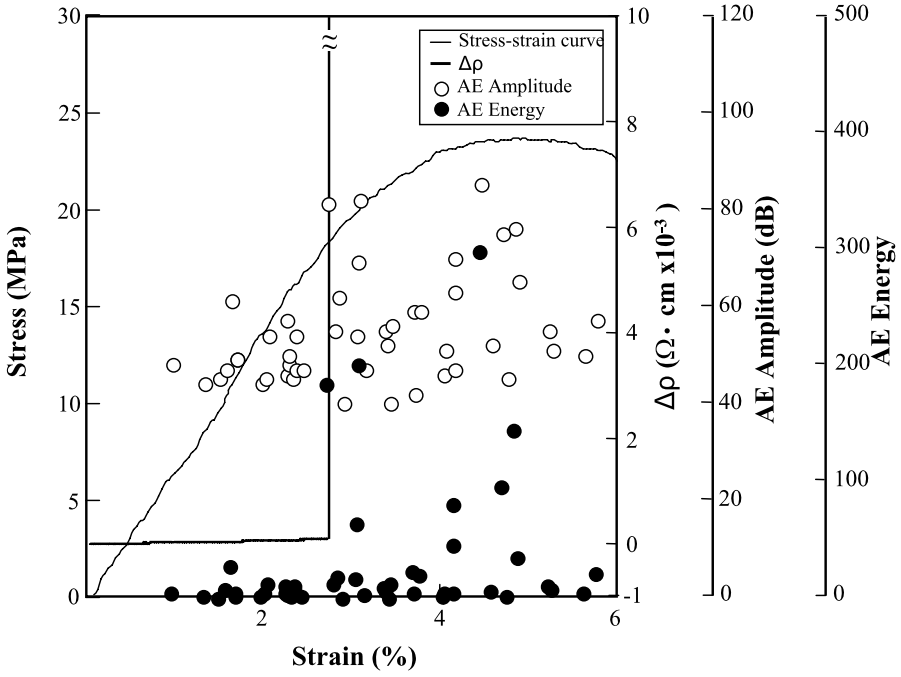

(c)

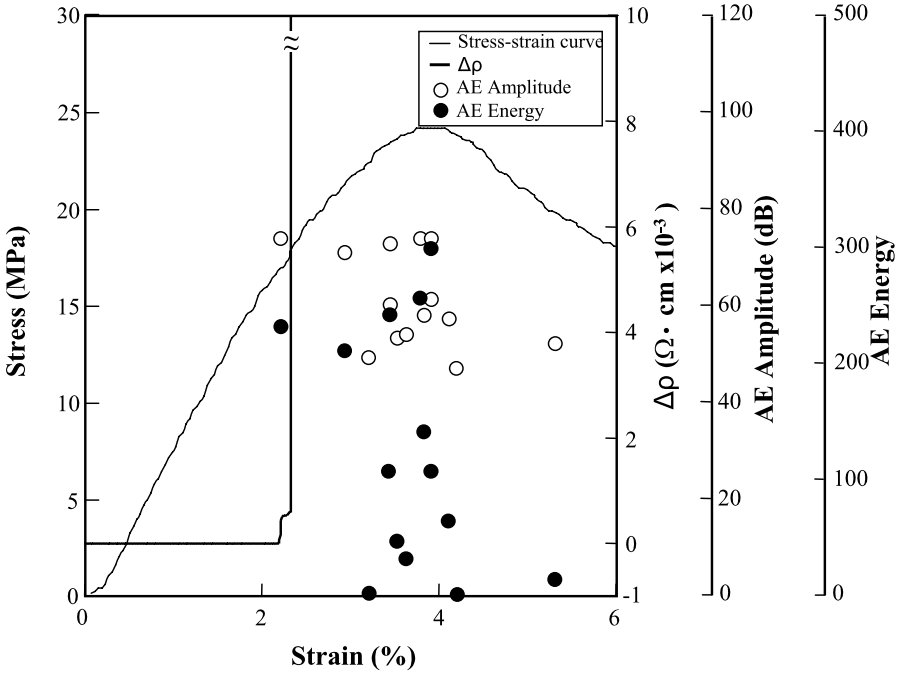

(d)

Figure 8. (Continued.)

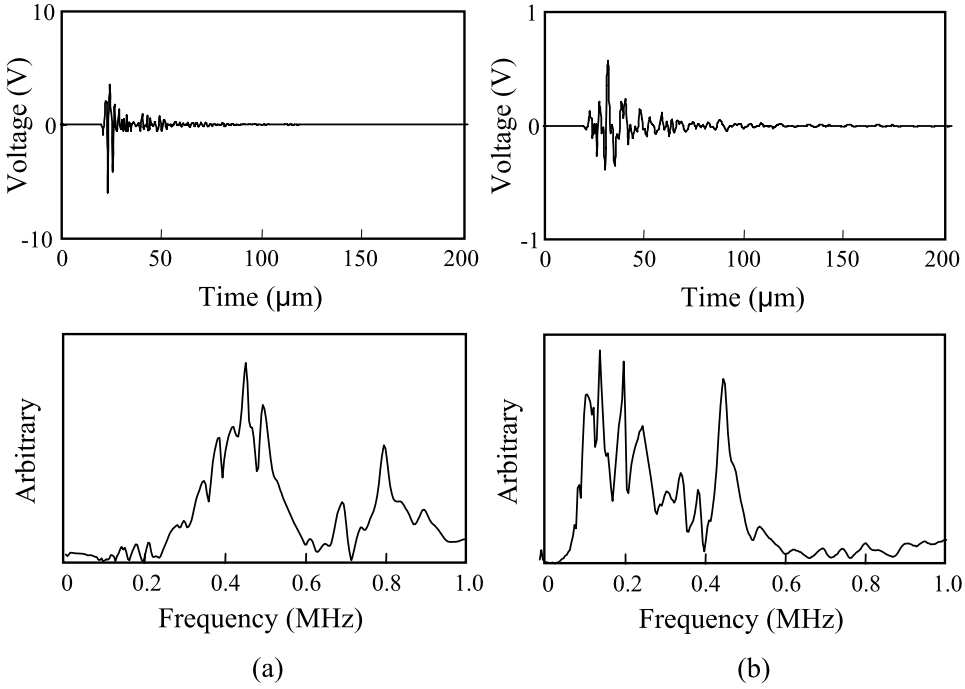

Figure 9. AE waveform and their FFT analysis of damage sensing for micro-carbon fiber/CNF–cement double-matrix composites by acoustic emission: (a) micro-carbon fiber fracture; (b) debonding or CNF–cement matrix cracking.

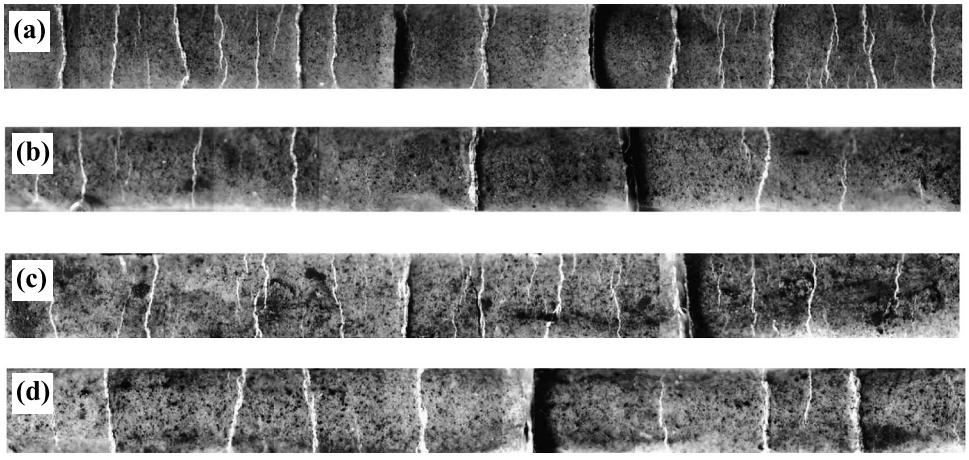

Figure 10. Photos of surfaces after AE test of micro-carbon fiber/CNF–cement double-matrix composites with CFN concentrations of: (a) 0 wt%; (b) 1 wt%; (c) 3 wt% and (d) 5 wt%.

CNF concentration, however, micro-carbon fiber fracture by just one large step was detected in the electrical resistivity as well as AE. As the second consequent micro-

carbon fiber fracture occurred, the electrical resistivity increased 'infinitely'. Since the percolation structure of CNF was developed poorly in cement, the less conductive CNF–cement composites became nonconductive composites disconnected by vertical micro-cracks. Typical waveform of vertical cement crack or micro-carbon fiber failure exhibited large amplitude AE signals, whereas the signals associated with interfacial failure between micro-carbon fiber and cement matrix were much smaller in amplitude. Load and micro-damage sensing were monitored in single carbon fiber embedded cement composites with results comparable with those from previous similar works in single carbon fiber embedded epoxy composites.

Acknowledgements

This work was financially supported from Yunhak Project by Korea Institute of Standard and Science (KRISS), 2006. Zuo Jia Wang is grateful to the second stage of BK21 program for supporting a fellowship.

References

1. S. Tsantzalis, P. Karapappas, A. Vavouliotis, S. Tsotra, P. A. Paipetis and V. Kostopoulos, Enhancement of the mechanical performance of an epoxy resin and fiber reinforced epoxy resin composites by the introduction of CNF and PZT particle at the microscale, *Composites Part A* **38**, 1076–1081 (2006).
2. B. A. Higgins and W. J. Brittain, Polycarbonate carbon nanofiber composites, *Europ. Polym. J.* **41**, 889–893 (2005).
3. K. T. Lau and D. Hui, The revolutionary creation of new advanced materials–carbon nanotube composites, *Composites Part B* **33**, 263–277 (2002).
4. F. Pervin, Y. Zhou, V. K. Ranggaari and S. Jeelani, Testing and evaluation on the thermal and mechanical properties of carbon nanofiber reinforced SC-15 epoxy, *Mater. Sci. Engng A* **405**, 246–254 (2005).
5. V. Kostopoulos, P. Tsotra, P. Karapappas, S. Tsantzalis, A. Vavouliotis, T. H. Loutas, A. Paipetis, K. Friedrich and T. Tanimoto, Mode I interlaminar fracture of CNF or/and PZT doped CFRPs *via* acoustic emission monitoring, *Compos. Sci. Technol.* **67**, 822–828 (2007).
6. P. C. Aitcin, Cements of yesterday and today, concrete of tomorrow, *Cem. Concr. Res.* **30**, 1349–1359 (2000).
7. B. Mather, Concrete durability, *Cem. Concr. Compos.* **26**, 3–4 (2004).
8. B. Han and J. Ou, Embedded piezoresistive cement-based stress/strain sensor, *Sensor and Actuators A* **138**, 294–298 (2007).
9. J. P. Ou, Some recent advances of intelligent health monitoring system for civil infrastructures in HIT, *Proc. SPIE* **5851**, 147–162 (2004).
10. K. P. Chong, Health monitoring of civil structures, *J. Intell. Mater. Syst. Struct.* **9–11**, 892–898 (1999).
11. D. D. L. Chung, Cement reinforced with short carbon fibers: a multifunctional material, *Composites Part B* **31**, 511–526 (2000).
12. P. Garces, L. G. Andion, I. Varga, G. Catala and E. Zornoza, Corrosion of steel reinforcement in structural concrete with carbon material addition, *Corrosion Sci.* **49**, 2557–2566 (2007).

13. G. Y. Li, P. M. Wang and X. H. Zhao, Mechanical behavior and microstructure of cement of incorporation surface-treated multi-walled carbon nanotubes, *Carbon* **6**, 1239–1245 (2005).
14. D. D. L. Chung and S. Wen, Carbon fiber-reinforced cement as a strain-sensing coating, *Cem. Concr. Res.* **31**, 665–667 (2001).
15. D. D. L. Chung, *Multifunctional Cement-Based Materials*. Marcel Dekker, New York, USA (2003).
16. X. Wang and D. D. L. Chung, Improving the bond strength between carbon fiber and cement by fiber surface treatment and polymer addition to cement mix, *Cem. Concr. Res.* **26**, 1007–1012 (1996).
17. J. M. Park, S. I. Lee, K. W. Kim and D. J. Yoon, Interfacial properties of electrodeposited carbon fibers/epoxy composites using electro-micromechanical technique and nondestructive evaluation, *J. Colloid Interf. Sci.* **237**, 80–90 (2001).
18. G. Sotiriadis, P. Tsotra, A. Paipetis, P. Karappapas, A. Vavouliotis and V. Kostopoulos, Fatigue damage behavior of glass fiber reinforced composites with and without carbon nanotubes matrix doping, in: *Non-destructive Damage Inspection*, pp. 123–127. TRANSFAC'06, San Sebastian, Spain (2006).
19. J. M. Park, E. M. Chong, D. J. Yoon and J. H. Lee, Interfacial properties of two SiC fiber-reinforced polycarbonate composites using the fragmentation test and acoustic emission, *Polym. Compos.* **19**, 747–757 (1998).
20. R. K. Verma, R. G. Kander and B. S. Hsiao, Acoustic emission monitoring of damage using high amplitude gains in carbon fiber reinforced polyetheretherketone, *J. Master. Sci. Lett.* **13**, 438–442 (1994).
21. B. T. Ma, L. S. Schadler, C. Laird and J. C. Figueroa, Acoustic emission in single filament carbon/polycarbonate and Kevlar/polycarbonate composite under tensile deformation, *Polym. Compos.* **11**, 211–216 (1990).
22. T. H. Loutas, V. Kostopoulos, C. Ramirez-Jimenez and M. Pharaoh, Damage evolution in center-holed glass/polyester composites under quasi-static loading using time/frequency analysis of acoustic emission monitored waveforms, *Compos. Sci. Technol.* **66**, 1366–1375 (2006).
23. V. Kostopoulos, T. Loutas and C. Dassios, Fracture behavior and damage mechanisms identification of SiC/glass ceramic composites using AE monitoring, *Compos. Sci. Technol.* **67**, 1740–1746 (2007).
24. J. M. Park, I. L. Lee, J. W. Kim and D. J. Yoon, Interfacial and microfailure evaluation of modified single fibers/brittle-cement matrix composites using electro-micromechanical technique and acoustic emission, *J. Coll. Interf. Sci.* **244**, 410–422 (2001).
25. J. M. Park, D. S. Kim, J. W. Kong, S. J. Kim, J. H. Jang, M. Y. Kim, W. H. Kim and K. L. DeVries, Interfacial evaluation and self-sensing on residual stress and microfailure of toughened carbon fiber/epoxy-amine terminated (AT)–polyetherimide (PEI) composites, *Composites Part B* **38**, 833–846 (2007).
26. S. Wang, S. I. Lee, D. D. L. Chung and J. M. Park, Load transfer from fiber to polymer matrix, studied by measuring the apparent elastic modulus of carbon fiber embedded in epoxy, *Compos. Interf. Lett.* **8**, 435–441 (2001).